scientific data

Check for updates

OPEN

DATA DESCRIPTOR

A ten-year numerical hindcast of hydrodynamics and sediment dynamics in the Loire Estuary

Florent Grasso ✉ & Matthieu Caillaud

A numerical hindcast of the macrotidal Loire Estuary (France) has been generated to provide a long-term dataset (2008–2018) of estuarine hydrodynamics, temperature, salinity, and sediment dynamics. This hindcast is based on simulations coupling water motion, wave and mixed sediment models, forced with realistic conditions and extensively validated in the salinity gradient and turbidity maximum areas. These data represent extremely valuable information for diverse scientific communities, providing (i) environmental parameters for ecosystemic studies along the Loire River–sea continuum, (ii) a singular estuarine configuration for inter-comparison of estuarine functioning, and (iii) a ten-year synoptical view of a major estuarine environment of the North Atlantic Ocean.

Background & Summary

Estuaries represent crucial interfaces along the land-sea continuum, impacted by marine, riverine, and atmospheric forcing. The mixing between freshwater and seawater strongly impacts the fate of dissolved and particulate matters between continental and marine environments (e.g., nutrients, contaminants and sediments)[1]. Moreover, estuarine circulation and tidal currents can induce high levels of suspended sediment concentration (SSC) and form estuarine turbidity maxima (ETM)[2–12], directly affecting estuarine morphodynamics and biogeochemical processes[13]. In addition to natural forcing, human-induced changes (e.g., estuary deepening and narrowing) have drastic impacts on the physical and ecological estuary functioning[14–18]. Exceptional hydro-meteorological conditions, associated with inter-annual variability and/or climate changes, exacerbate drought, flood and stormy periods that have a major impact on estuary physics. Therefore, it is essential to understand the estuarine dynamics during such critical periods (from events to years) to be able to provide insights into estuary trajectories under future climatic and human pressures[15].

Recent developments in realistic numerical models, i.e., based on realistic bathymetry and forcing conditions, enable hindcasts to be generated over decadal periods[15]. Such multi-year simulations, validated with long-term *in-situ* high-frequency monitoring networks[9,19,20], provide valuable four-dimensional parameters (i.e., horizontal, vertical, and temporal components) of environmental conditions, such as water level and current, temperature, salinity, SSC, and bed substrate composition. Such hindcasts are especially useful: (i) to study the impacts of anthropogenic and climate changes on estuarine physics and ETM dynamics;[11,15,16,21–23] and (ii) to provide abiotic explanatory parameters for biogeochemical and ecological studies[24–27].

Numerical hindcasts have recently been realised for two of the three largest French estuaries (Seine[15] and Gironde[21]), arousing interdisciplinary studies and tackling challenges on habitats and species distributions[24–26]. The aim of this study is to complete these datasets with a ten-year hindcast (2008–2018) for the Loire Estuary (France; Figs. 1, 2). On the one hand, it offers environmental parameters for ecosystemic studies along the Loire River–sea continuum; and on the other hand, it provides a contrasted estuarine configuration for inter-estuary comparisons[5,28–32].

The Loire Estuary is the second largest French estuary, extending 100 km from Saint Florent-le-Vieil at the upstream limit of tidal influence to the Bay of Biscay on the Atlantic Coast (Fig. 1a,b). The estuary has a semi-diurnal macrotidal regime with a tidal range varying from 1.5 to 6.4 m at Saint Nazaire close to the estuary mouth (Fig. 1c). Tides and river flow induce large seasonal, fortnightly, and semi-diurnal salinity changes[27]. Moreover, the Loire Estuary is characterized by a well-developed turbidity maximum (i.e., SSC exceeding 0.5 g/l at the surface and ETM mass up to 1 Mt)[9], migrating from Nantes to Donges during low to high river discharges

Ifremer – DYNECO/DHYSED, Centre de Bretagne, CS 10070, Plouzané, F-29280, France. ✉e-mail: florent.grasso@ifremer.fr

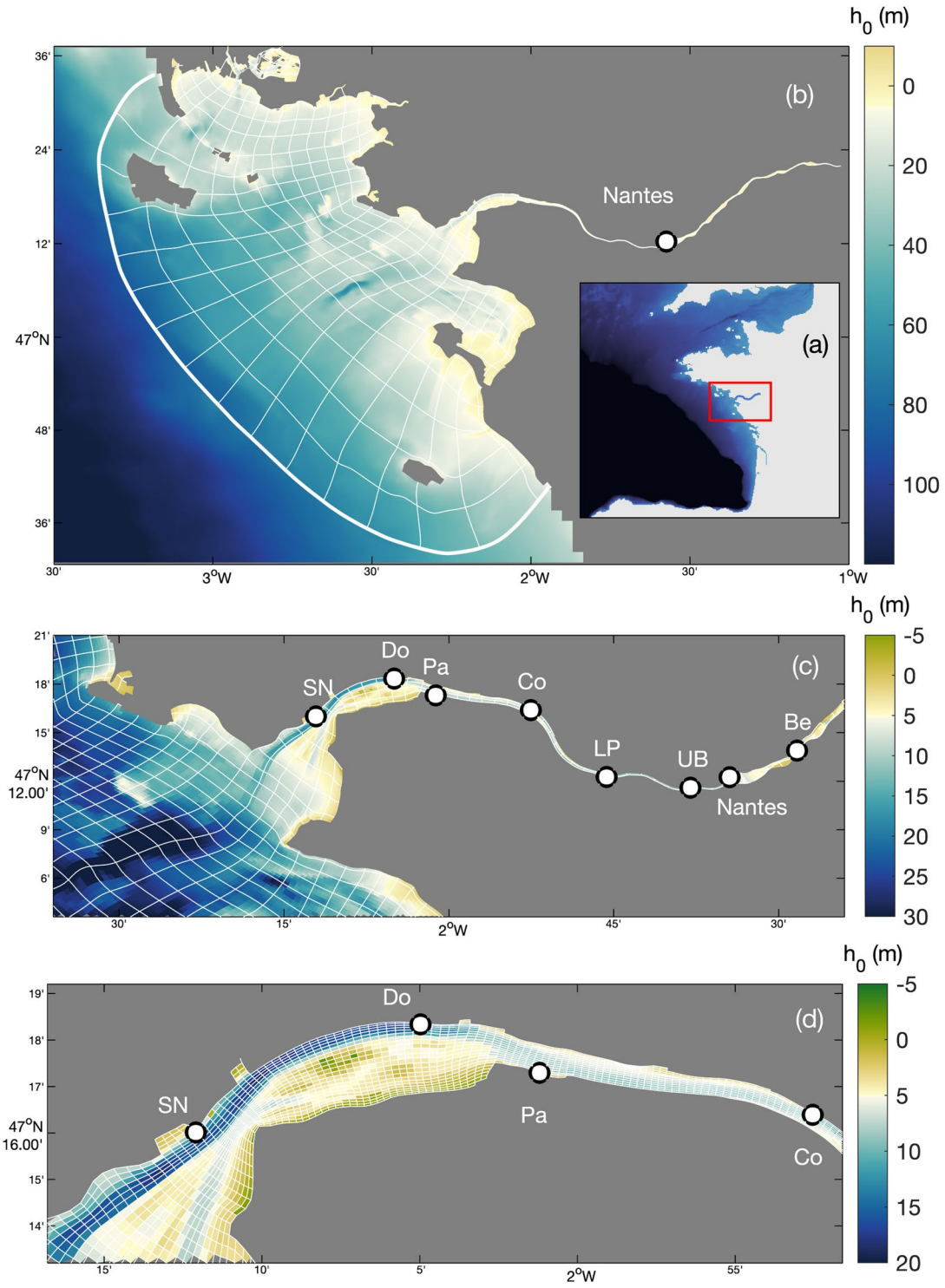

Fig. 1 Bathymetry of the Loire Estuary, France (with h_0 the water depth relative to mean sea level). (**a**) Location of the estuary in the Bay of Biscay (Western French Atlantic Coast), (**b**) full domain of the MARS3D model with every tenth grid cell represented, (**c**) focus on the estuary with every fifth grid cell represented, and (**d**) focus on the lower estuary with every grid cell represented. Black circles represent locations of water level, salinity, and SSC comparisons: Saint Nazaire 'SN', Donges 'Do', Paimboeuf 'Pa', Cordemais 'Co', Le Pellerin 'LP', Usine Brulée 'UB', and Bellevue 'Be'.

(Fig. 1c,d). Between 2009 and 2018, the Loire River discharge ranged from 100 to 3700 m^3/s, with a mean freshwater runoff of around 730 m^3/s and a terrigenous sediment load of around 1.1 Mt/year.

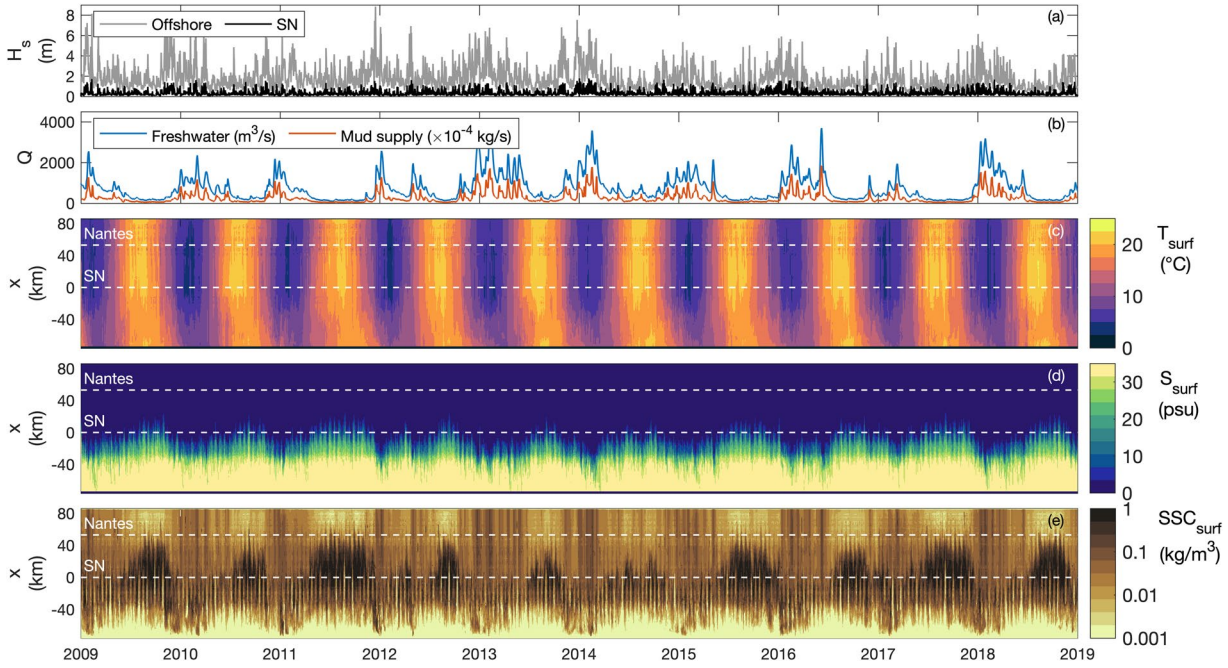

Fig. 2 Numerical hindcast of the Loire Estuary (2009–2018). (**a**) Significant wave height H_s at the offshore model boundary (grey) and at Saint Nazaire 'SN' (black), and (**b**) Loire River discharge Q at the upstream model boundary for freshwater (blue) and mud supply (orange). Width-averaged along-estuary transects of surface: (**c**) temperature T_{surf}, (**d**) salinity S_{surf}, and (**e**) suspended sediment concentration SSC_{surf}. In (**c**–**e**), white-dashed lines represent Saint Nazaire 'SN' and Nantes locations, at x = 0 and 53 km respectively.

Methods

A realistic three-dimensional numerical model has been set up to simulate the hydrodynamics, temperature, salinity, and sediment dynamics along the Loire Estuary. Similar models have previously been implemented in the Seine[11,15,16,22,23,25,33] and Gironde[21,24,26] estuaries (France). Hereafter is presented an overview of the model characteristics both in terms of hydrodynamics and sediment transport.

Hydrodynamic model. The model is based on a non-nested (i.e., unique) configuration using the hydrostatic model MARS3D[34]. An orthogonal curvilinear grid is used to better represent the estuarine shape and to optimize computational costs while refining the grid resolution in some specific areas (i.e., in the river meanders, in the central estuary, and at the estuarine mouth; Fig. 1). Horizontal cell size ranges from around 50 m in the meanders to approximately 1.3 km offshore while the vertical grid is divided into 10 equidistant sigma layers.

The 114 main tidal components, extracted from the CST France database, https://maree.shom.fr (Service Hydrographique et Océanographique de la Marine, SHOM), are used to force the circulation at the open boundaries. Surges, provided by a configuration of the two-dimensional MARS2D model applied to a larger domain (i.e., over the Bay of Biscay), are added to the water elevation at these same boundaries. Realistic freshwater discharges and sediment loads are prescribed at the upstream boundary of the Loire River (i.e., Saint Florent-le-Vieil) and at the Vilaine Estuary mouth for the Vilaine River (see further details on river supplies in the "Data records" section). In addition, the model is forced by wind stresses and pressure gradients obtained from the high-resolution meteorological AROME model (Météo-France): https://donneespubliques.meteofrance.fr. The simulated turbulence is based on a k-ε turbulence closure scheme. Waves are simulated with the WAVEWATCH III® (WW3) numerical model[35] using the same computational grid as the one used by MARS3D in this study. The hourly free surface elevation and current velocity provided by the MARS3D hydrodynamic model, along with local winds and swell data extracted from a larger model, were used to force the WW3 configuration. However, the wave effects on hydrodynamic circulation are not taken into account because of the dominance of tidal currents over wave-induced currents. The bottom orbital velocities simulated by the wave model were used to compute the wave-induced bed shear stress. Finally, the total bed shear stress (τ) was expressed as a combination of the current-induced and wave-induced bed shear stresses, accounting for non-linear interactions following the formulation of Soulsby[36].

The hydrodynamic bottom roughness z_{0b} is spatially distributed according to the observed sediment substrate. However, the sediment nature in the estuary changes according to the ETM location and the presence of fluid mud layers, which depend on the Loire River discharge. Therefore, following an approach adopted by ARTELIA[37], the bottom roughness also depends on the Loire River discharge[38]. More details on the hydrodynamic model configuration are provided by Khojasteh Pour Fard[39].

Particle diameter		*Gravel*	1 mm	*Based on local granulometric data*
		Medium sand	450 µm	
		Fine sand	200 µm	
		Very fine sand	100 µm	
		Mud	<63 µm	
Mud settling velocity (Eq. 1)		$w_{s,min}$	0.1 mm/s	
		$w_{s,max}$	1 mm/s	
		c_1	0.003	
		c_2	0.79	
		a	0.3	
		b	0.18	
Erosion law	Non-cohesive	n_{sand}	1.6	
	Cohesive	n_{mud}	1	
		$E_{0,mud}$	10^{-3}	
		α_1	10^{-5}	
		α_2	2	

Table 1. Main sediment model calibration parameters.

Stations			SN	Do	Pa	Co	LP	UB	Be
Water level	ζ	r^2	**0.99** 0.99	**0.98** 0.99		**0.97** 0.97	**0.97** 0.98	**0.96** 0.97	
		e_{rms} (m)	**0.15** 0.14	**0.20** 0.16		**0.26** 0.25	**0.23** 0.22	**0.27** 0.24	
		b (m)	**−0.02** 0.00	**0.00** −0.06		**0.02** 0.03	**−0.04** −0.05	**−0.01** −0.04	
Surface salinity	Sal_{hf}	r^2			**0.91** 0.79		**0.69** 0.65		
		e_{rms} (psu)			**2.6** 3.5		**0.5** 0.5		
		b (psu)			**−1.7** 0.7		**−0.3** −0.1		
	Sal_{tide}	r^2			**0.96** 0.91		**0.73** 0.78		
		e_{rms} (psu)			**1.9** 1.9		**0.4** 0.3		
		b (psu)			**−1.6** 0.6		**−0.3** −0.1		
Surface suspended sediment concentration	SSC_{hf}	r^2			**0.12** 0.09	**0.14** 0.42	**0.29** 0.3		**0.35** 0.38
		e_{rms} (kg/m^3)			**1.10** 0.49	**1.07** 0.56	**0.59** 0.75		**0.03** 0.008
		b (kg/m^3)			**−0.38** 0.00	**−0.41** −0.12	**−0.21** −0.30		**0.01** −0.01
	SSC_{tide}	r^2			**0.40** 0.19	**0.51** 0.87	**0.71** 0.65		**0.42** 0.41
		e_{rms} (kg/m^3)			**0.61** 0.31	**0.77** 0.32	**0.47** 0.59		**0.03** 0.05
		b (kg/m^3)			**−0.40** −0.02	**−0.42** −0.12	**−0.21** −0.31		**0.01** −0.01

Table 2. Numerical model skills (i.e., correlation coefficient r^2, root mean square error e_{rms}, and bias b) for water level, salinity and SSC at Bellevue 'BE', Usine Brulée 'UB', Le Pellerin 'LP', Cordemais 'Co', Paimboeuf 'Pa', Donges 'Do', and Saint Nazaire 'SN'. Bold and normal font type values correspond to the 2008 and 2018 simulations, respectively. 'hf' and 'tide' subscripts define high-frequency (i.e., every 30 minutes) and tide-averaged values, respectively.

Sediment transport model. The hydrodynamic model is coupled with the process-based, multiclass, multilayer sediment transport model MUSTANG[40–42], which computes the temporal and spatial variations of sand and mud content in the bed under hydrodynamic forces and consolidation process. The MARS3D-MUSTANG coupling resolves advection-diffusion equations in the water column and sediment exchanges between the bed and the water column for different particle classes. Based on hundreds of granulometric samples collected in the Loire Estuary[43], five sediment classes are prescribed in this hindcast: one mud, three sands, and one gravel (see sediment class diameters in Table 1). Sediment classes are initially distributed according to bed substrate observations from the SHOM.

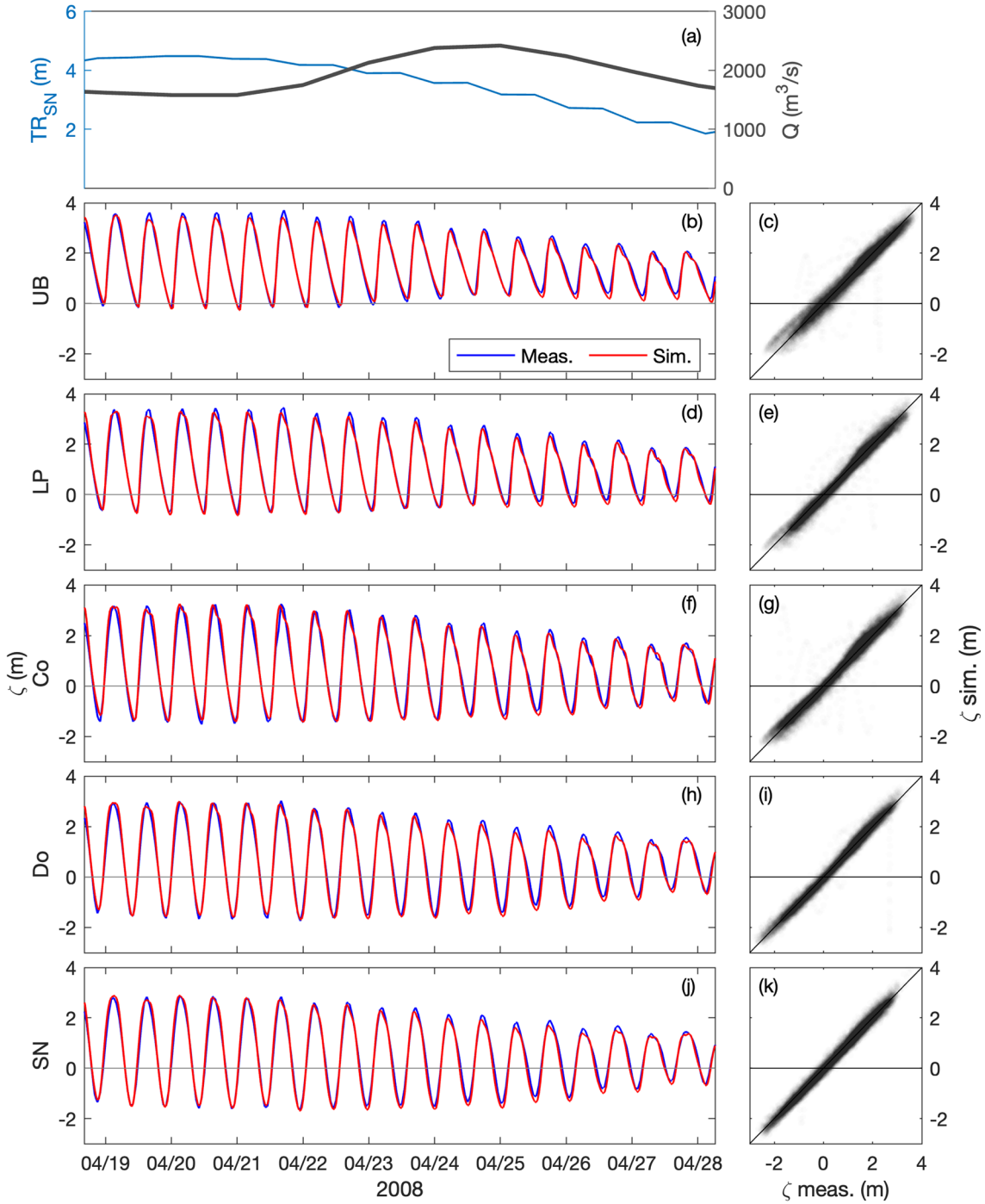

Fig. 3 Hindcast validation of water levels ζ along the Loire Estuary. (**a**) Loire River discharge Q at the upstream model boundary and tidal range TR_{SN} at Saint Nazaire 'SN' (blue). Water surface elevations at (**b,c**) Usine Brulée 'UB', (d-e) Le Pellerin 'LP', (**f,g**) Cordemais 'Co', (**h,i**) Donges 'Do', and (**j,k**) Saint Nazaire 'SN' (see station locations in Fig. 1c). (Left panels) Measurements (blue) and simulations (red) from April 19 to 28, 2008. (Right panels) simulations versus measurements from January to December 2008.

Non-cohesive sediment classes (sands and gravel) have constant settling velocities depending on their diameters[36]. The coarser classes are transported in the bottom layer only, except for the very fine sand, which was treated in three dimensions. In two dimensions, the velocity in the bottom layer is corrected to account for a logarithmic profile for the velocity in the whole water column, and the calculated sand concentration is then assumed to follow a Rouse profile[44]. The mud class is computed as a three-dimensional variable with a settling velocity $w_{s,mud}$ varying with concentration and turbulence to represent flocculation processes following van Leussen[45]:

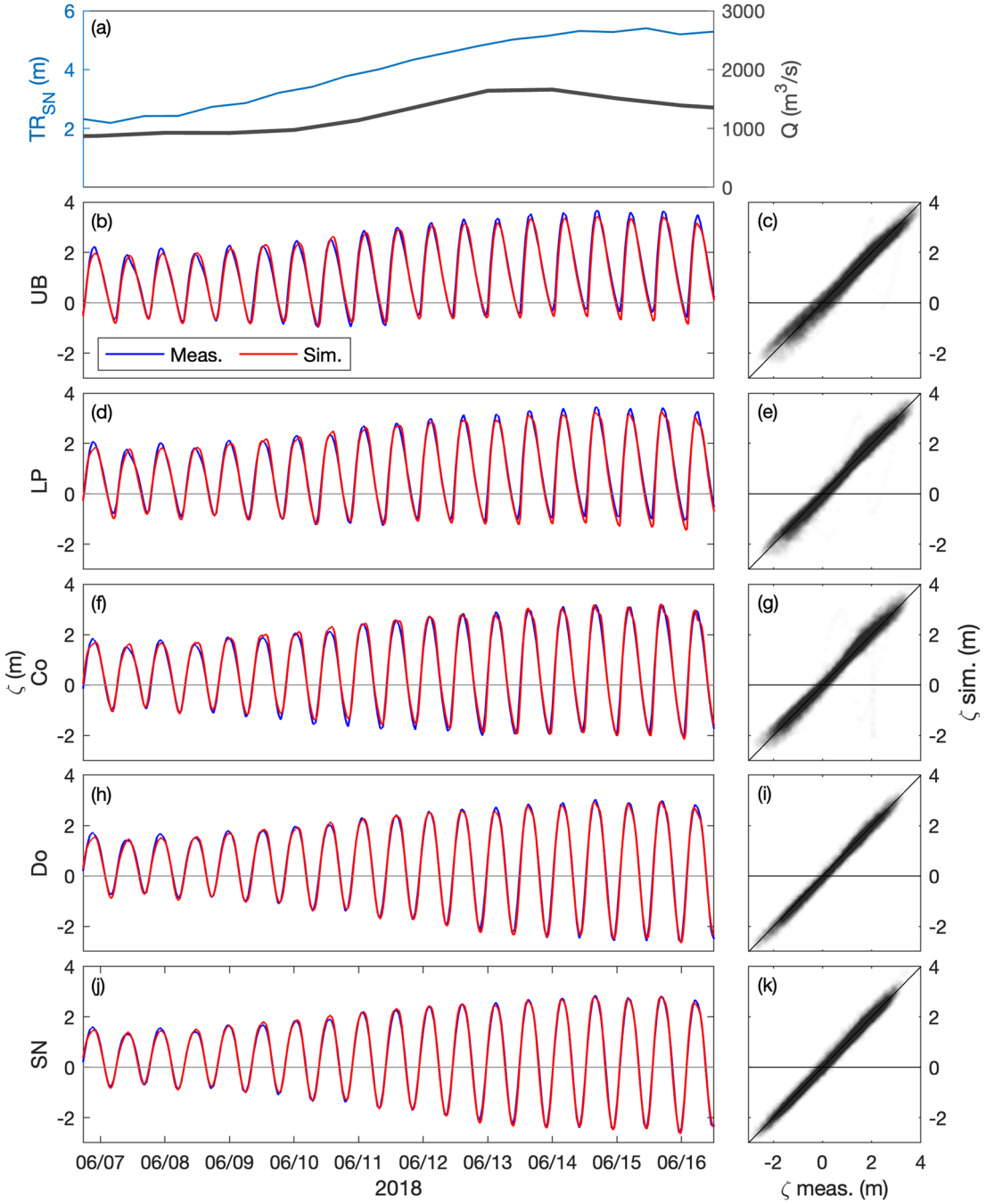

Fig. 4 Hindcast validation of water levels ζ along the Loire Estuary. (**a**) Loire River discharge *Q* at the upstream model boundary and tidal range TR_{SN} at Saint Nazaire 'SN' (blue). Water surface elevations at (**b,c**) Usine Brulée 'UB', (**d,e**) Le Pellerin 'LP', (**f,g**) Cordemais 'Co', (**h,i**) Donges 'Do', and (**j,k**) Saint Nazaire 'SN' (see station locations in Fig. 1c). (Left panels) Measurements (blue) and simulations (red) from June 7 to 16, 2018. (Right panels) simulations versus measurements from January to December 2018.

$$w_{s,mud0} = \min\left[w_{s,max}, \max\left(w_{s,min}, c_1 . C_{mud}^{c_2} . \frac{1 + aG}{1 + bG^2}\right)\right] \quad (1)$$

with C_{mud} the mud concentration (kg/m^3), *G* the turbulent shear rate (s^{-1}), and $w_{s,min}$, $w_{s,max}$, *a*, *b*, c_1, c_2 calibration parameters detailed in Table 1. A dependency between the mud settling velocity and salinity (*S*) is also considered to account for the influence of salinity on flocculation[46]: below a critical salinity of 5 psu, the mud settling velocity decreases with salinity (see details in Diaz, *et al.*[21]).

The erosion flux is based on Partheniades-Arathurai equation[47]:

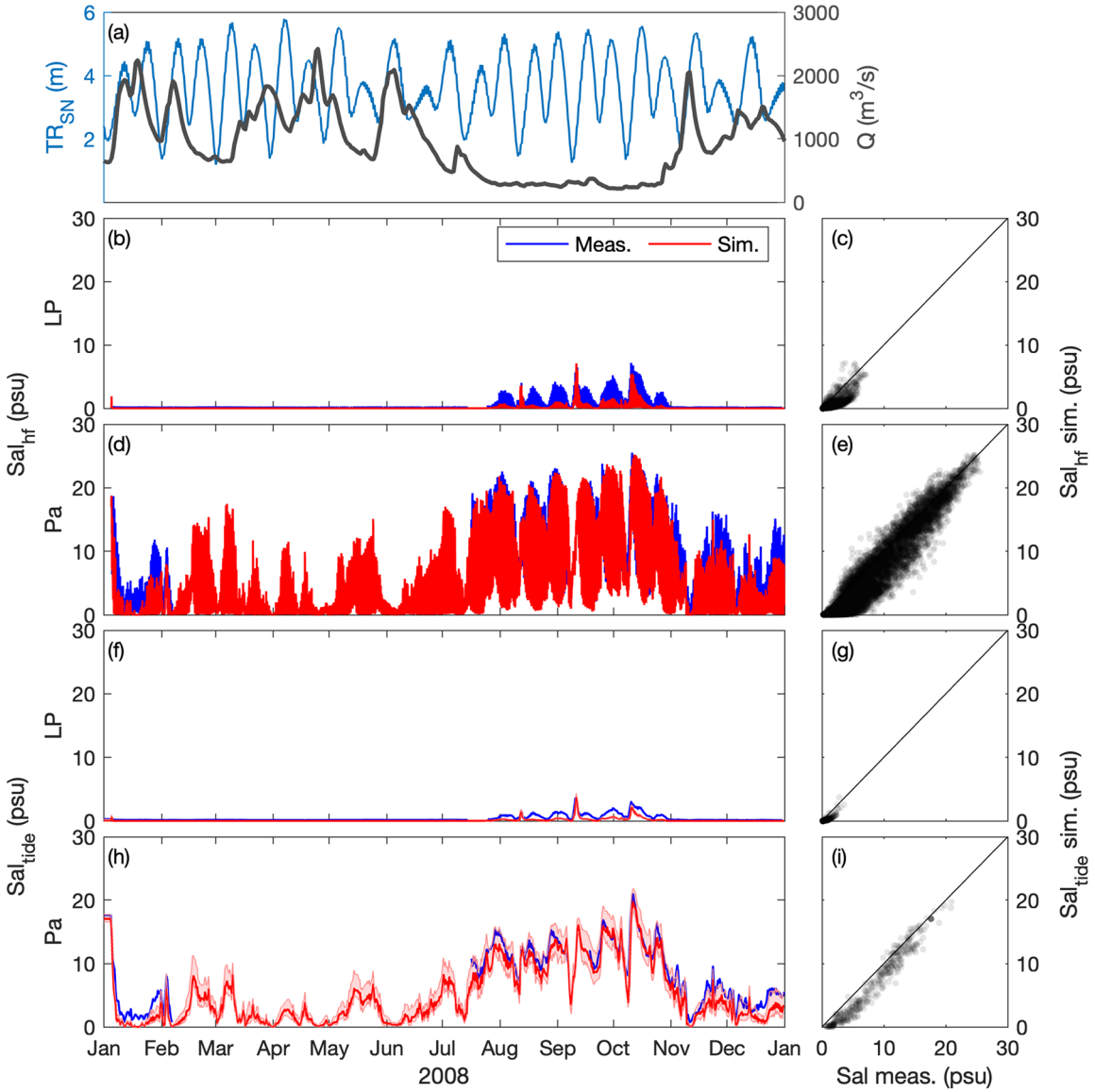

Fig. 5 Hindcast validation of salinity *Sal* along the Loire Estuary. (**a**) Loire River discharge *Q* at the upstream model boundary and tidal range TR_{SN} at Saint Nazaire 'SN' (blue). Surface salinity at (**b,c,f,g**) Le Pellerin 'LP' and (**d,e,h,i**) Paimboeuf 'Pa' (see station locations in Fig. 1c). (Left panels) Measurements (blue) and simulations (red), and (right panels) simulations versus measurements, from January to December 2008. (**b**–**e**) High-frequency salinity Sal_{hf} (i.e., every 30 minutes) and (**f**–**i**) tide-averaged salinity Sal_{tide}.

$$\begin{cases} \tau > \tau_{ce} \Rightarrow E = E_0 \left(\dfrac{\tau}{\tau_{ce}} - 1 \right)^n \\ \tau < \tau_{ce} \Rightarrow E = 0 \end{cases} \quad (2)$$

with E the erosion flux, E_0 an erodibility parameter (kg/m²/s), τ_{ce} the critical shear stress for erosion (N/m²), and n a calibration parameter. A distinction between cohesive and non-cohesive sediment behaviours are made based on the mud fraction in the bed surficial layer (f_m). In both cases, the Partheniades equation was prescribed with different calibration parameters. For a non-cohesive behaviour ($f_m < f_{m,cr1}$ where $f_{m,cr1} = 1000.d_{50,sand}$, with $d_{50,sand}$ the weighted mean diameter of sand classes in the surficial layer), the erosion regime follows a pure sand behaviour. The critical shear stress for erosion is determined by the Shields criteria[36], the erosion rate is derived from erodibility measurements[48], and the calibration parameter n is defined as n_{sand} (Table 1). In the presence of a cohesive seabed ($f_m > 0.7$; Le Hir, *et al.*[41]), the formulation follows a pure mud erosion regime with $n = n_{mud}$ and $E = E_{0,mud}$ (Table 1). The critical shear stress for mud erosion $\tau_{ce,mud}$ depends on the bed consolidation state, which is represented by the relative mud concentration (C_{relmud}) through a classical

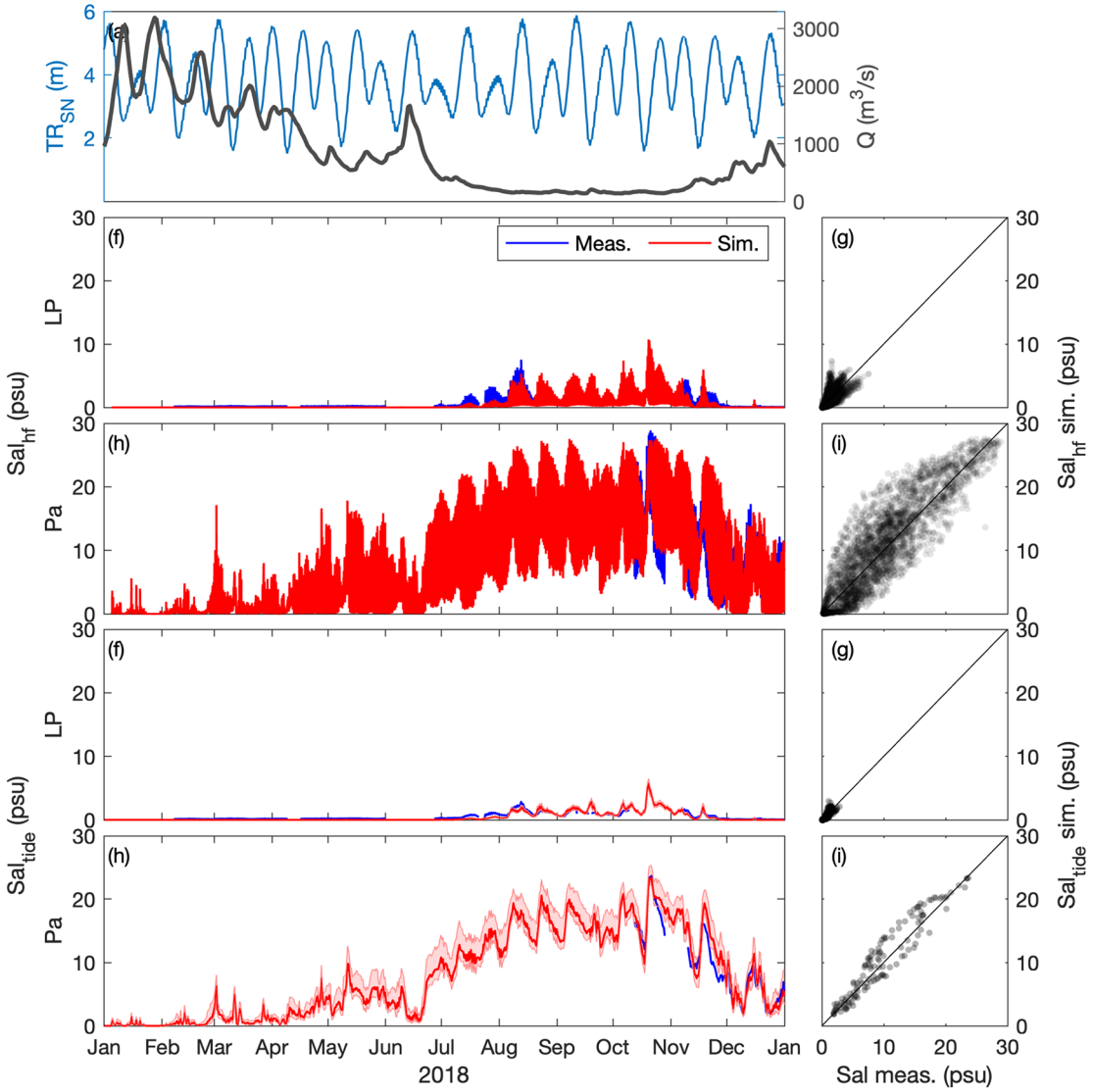

Fig. 6 Hindcast validation of salinity *Sal* along the Loire Estuary. (**a**) Loire River discharge *Q* at the upstream model boundary and tidal range TR_{SN} at Saint Nazaire 'SN' (blue). Surface salinity at (**b,c,f,g**) Le Pellerin 'LP' and (**d,e,h,i**) Paimboeuf 'Pa' (see station locations in Fig. 1c). (Left panels) Measurements (blue) and simulations (red), and (right panels) simulations versus measurements, from January to December 2018. (**b**–**e**) High-frequency salinity Sal_{hf} (i.e., every 30 minutes) and (**f**–**i**) tide-averaged salinity Sal_{tide}.

power law $\tau_{ce,mud} = \alpha_1 . C_{relmud}{}^{\alpha 2}$ (see Grasso, *et al.*[40]), with α_1 and α_2 defined in Table 1. Here, C_{relmud} is defined as the mud concentration in the space between sand particles[49]. Finally, for a mixed erosion regime, the erosion law parameters are linearly interpolated between pure sand and pure mud behaviours. The main empirical parameters are identified in Table 1 and further details on the formulations used in this model can be found in Grasso, *et al.*[11] and Diaz, *et al.*[21].

The deposition flux is calculated using a critical shear stress for deposition for each sediment class following the law of Krone[11,21,41,50]. Sediment sliding along the slope is taken into account to prevent an excessive increase of bed slope between depositing banks and the eroding channel. This process is computed by assigning a part of the deposition flux from one cell to the neighbouring one based on the slope between the two cells. The fraction of fresh deposit transposed to a deeper adjacent cell linearly depends on the local slope.

Hindcast simulations over the 2008–2018 period were run through independent years following a morphostatic approach, i.e., no morphodynamic coupling, which is relevant when morphological changes remain relatively small to hydrodynamic processes[15]. This assumption holds for the 2008–2018 period because the Loire Estuary is heavily dredged at a constant depth and no significant changes have been observed in the bathymetry since 2000[9,29]. This is confirmed by the model validation presenting similar skills in 2008 and 2018 (Table 2). Each year was run twice to consider a 1-year spin-up period before analysing the half-hourly outputs[11,16,23].

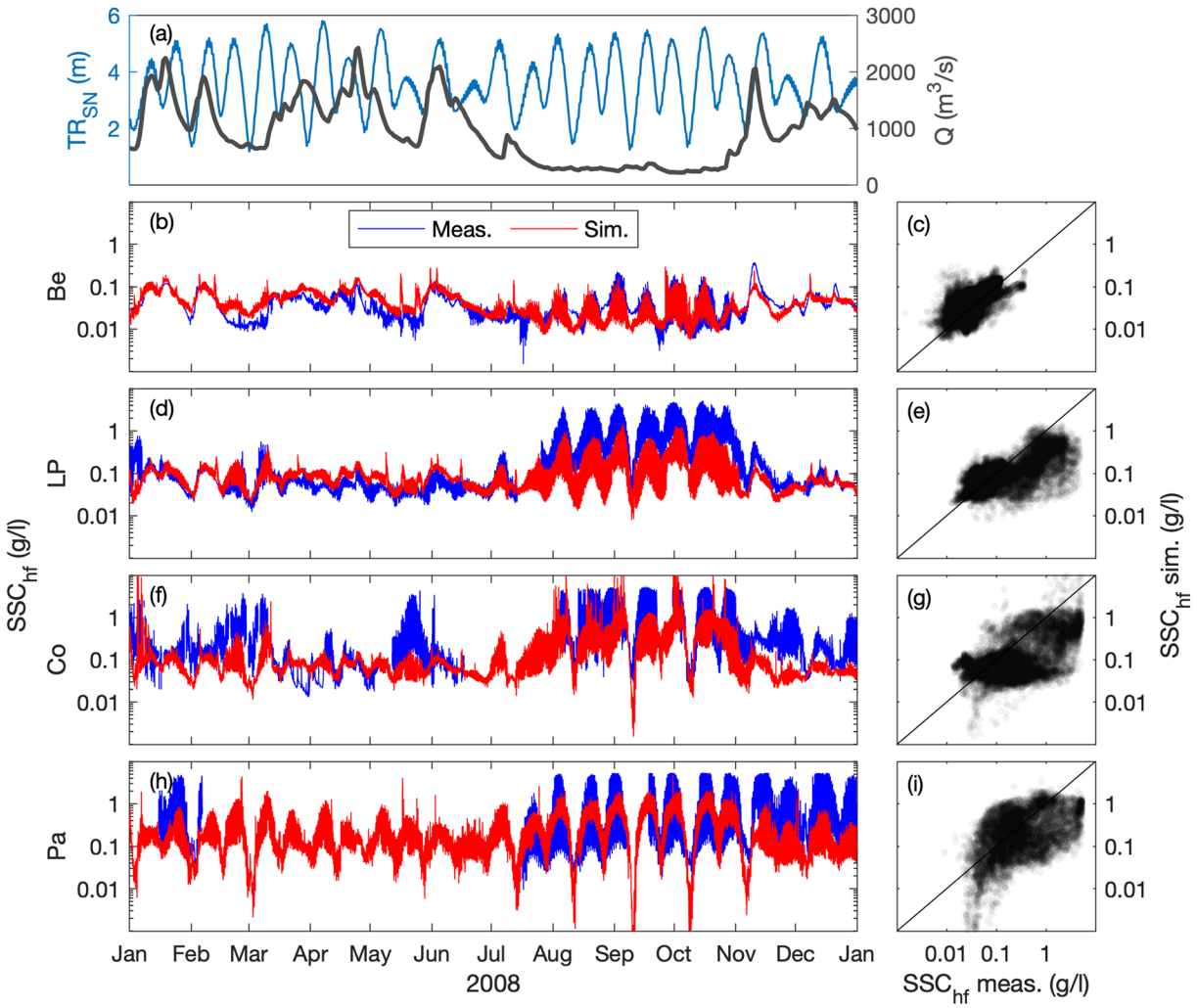

Fig. 7 Hindcast validation of high-frequency suspended sediment concentration SSC_{hf} along the Loire Estuary. (**a**) Loire River discharge Q at the upstream model boundary and tidal range TR_{SN} at Saint Nazaire 'SN' (blue). Surface SSC_{hf} at (**b,c**) Bellevue 'Be', (**d,e**) Le Pellerin 'LP', (**f,g**) Cordemais 'Co', and (**h,i**) Paimboeuf 'Pa' (see station locations in Fig. 1c). (Left panels) Measurements (blue) and simulations (red), and (right panels) simulations versus measurements, from January to December 2008.

Data Records

Hindcast repository. The data files containing the results of the Loire Estuary hindcast, i.e., hydrodynamics, temperature, salinity, and sediment dynamics, are available on the CurviLoire Hindcast repository[51].

The repository is structured in four directories:

- /hydro (NetCDF files): 3D half-hourly results for water column variables:
  - Hydrodynamics: water depth '*H0*', water level '*XE*', horizontal current velocity '*U,V*';
  - Temperature '*TEMP*', salinity '*SAL*';
  - Waves: significant height '*hs*', direction '*dir*', bottom orbital velocity '*ubrx,ubry*';
  - Suspended sediment concentration: mud '*Mud*', very fine sand '*Veryfinesand*', fine sand '*Finesand*', medium sand '*Mediumsand*', and gravel '*Gravel*'.
- /sedim (NetCDF files): 3D half-hourly results for bed compartment variables:
  - Bed shear stress: wave-induced '*TENFONW*', current-induced '*TENFONC*', and total components '*TENFON*';
  - Sediment bed: total thickness '*EPTOT*', number of layers '*NBNIV*', layer thickness '*DZS*';
  - Bed sediment concentration: mud '*Mud*', very fine sand '*Veryfinesand*', fine sand '*Finesand*', medium sand '*Mediumsand*', and gravel '*Gravel*'.

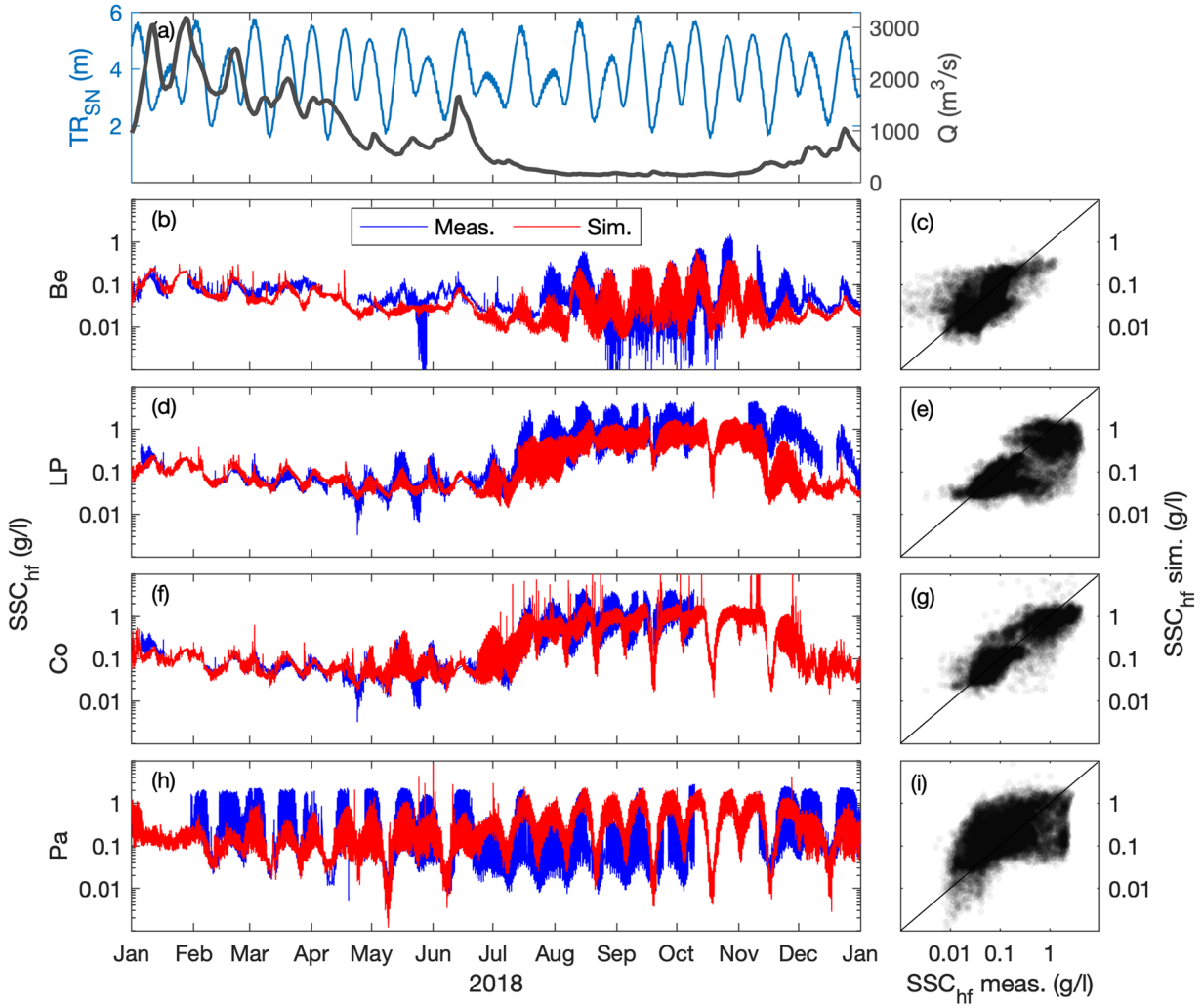

Fig. 8 Hindcast validation of high-frequency suspended sediment concentration SSC_{hf} along the Loire Estuary. (**a**) Loire River discharge Q at the upstream model boundary and tidal range TR_{SN} at Saint Nazaire 'SN' (blue). Surface SSC_{hf} at (**b,c**) Bellevue 'Be', (**d,e**) Le Pellerin 'LP', (**f,g**) Cordemais 'Co', and (**h,i**) Paimboeuf 'Pa' (see station locations in Fig. 1c). (Left panels) Measurements (blue) and simulations (red), and (right panels) simulations versus measurements, from January to December 2018.

- /source_code (fortran files): the MARS3D-MUSTANG source codes used to provide the hindcast;
- /param_files (ascii files): the parameter files used to configure the simulations.

Hindcast forcing conditions. The hindcast gathers eleven individual years of simulations (from 2008 to 2018) with the following forcing conditions:

- Bathymetry: 2008;
- Atmospheric forcing: Météo-France AROME ($1.3 \times 1.3\,km^2$ spatial resolution and hourly outputs);
- Open boundary conditions:
  - Tides: 114 main tidal components extracted from the CST France database (SHOM);
  - Storm surges: MARS2D-MANGAE2500 ($2.5 \times 2.5\,km^2$ spatial resolution and hourly outputs);
  - Waves: WAVEWATCH III®-NORGASUG 4 ($5 \times 5\,km^2$ spatial resolution and hourly outputs).
- River discharge:
  - Freshwater: daily-measured runoffs of the Loire and Vilaine rivers (Q_L and Q_V, respectively);
  - Sediment load: suspended mud concentration (SMC, in g/l) associated with the river runoff following the following relationships:

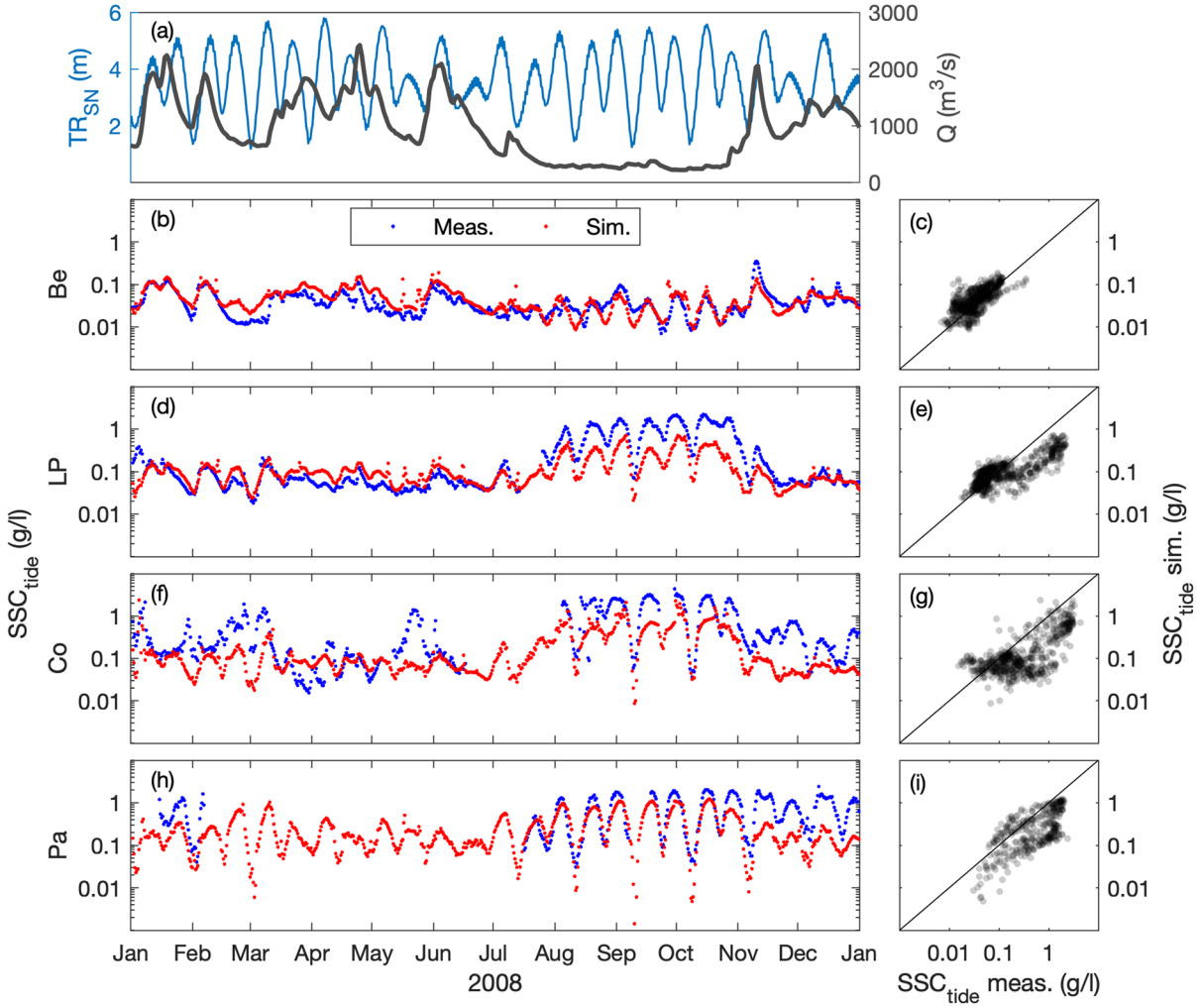

Fig. 9 Hindcast validation of tide-averaged suspended sediment concentration SSC_{tide} along the Loire Estuary. (**a**) Loire River discharge Q at the upstream model boundary and tidal range TR_{SN} at Saint Nazaire 'SN' (blue). Surface SSC_{tide} at (**b,c**) Bellevue 'Be', (**d,e**) Le Pellerin 'LP', (**f,g**) Cordemais 'Co', and (**h,i**) Paimboeuf 'Pa' (see station locations in Fig. 1c). (Left panels) Measurements (blue) and simulations (red), and (right panels) simulations versus measurements, from January to December 2008.

- Vilaine[52]: $SMC_V = (0.031 * Q_V + 17)/1000$
- Loire[37]:
$$\begin{cases} \text{Normal conditions: } SMC_L = \max(5,\ 0.036 * Q_L)/1000 \\ \text{Flood increase: } SMC_L = \max(5,\ 0.05 * Q_L)/1000 \\ \text{Flood decrease: } SMC_L = \max(5,\ 0.023 * Q_L)/1000 \end{cases}$$

Technical Validation

The numerical hindcast has been validated with the water level, salinity and SSC measurements in 2008 and 2018 provided by the GIP Loire Estuaire in the framework of the SYVEL high-frequency continuous monitoring network: https://www.loire-estuaire.org/accueil/nos-outils/reseau-de-mesures-en-continu-syvel-2. Simulations are compared after a one-year spin-up period.

Water level. Free surface elevation is compared at five tidal gauges along the estuary, where the salt wedge and turbidity maximum take place (i.e., Saint Nazaire 'SN', Donges 'Do', Cordemais 'Co', Le Pellerin 'LP', and Usine Brulée 'UB'; Fig. 1c). Measured and simulated water levels are presented over a spring-neap tidal cycle in April 2008 and June 2018, illustrating the tidal propagation from Saint Nazaire to Usine Brulée (left panels in Figs. 3, 4). The model properly simulates the tidal variations and correctly captures the tidal asymmetries along the estuary. Comparisons over the entire years (right panels in Figs. 3, 4) provide good agreements with correlation coefficients $r^2 \leq 0.96$ and root mean square errors $e_{rms} \leq 0.27$ m (Table 2).

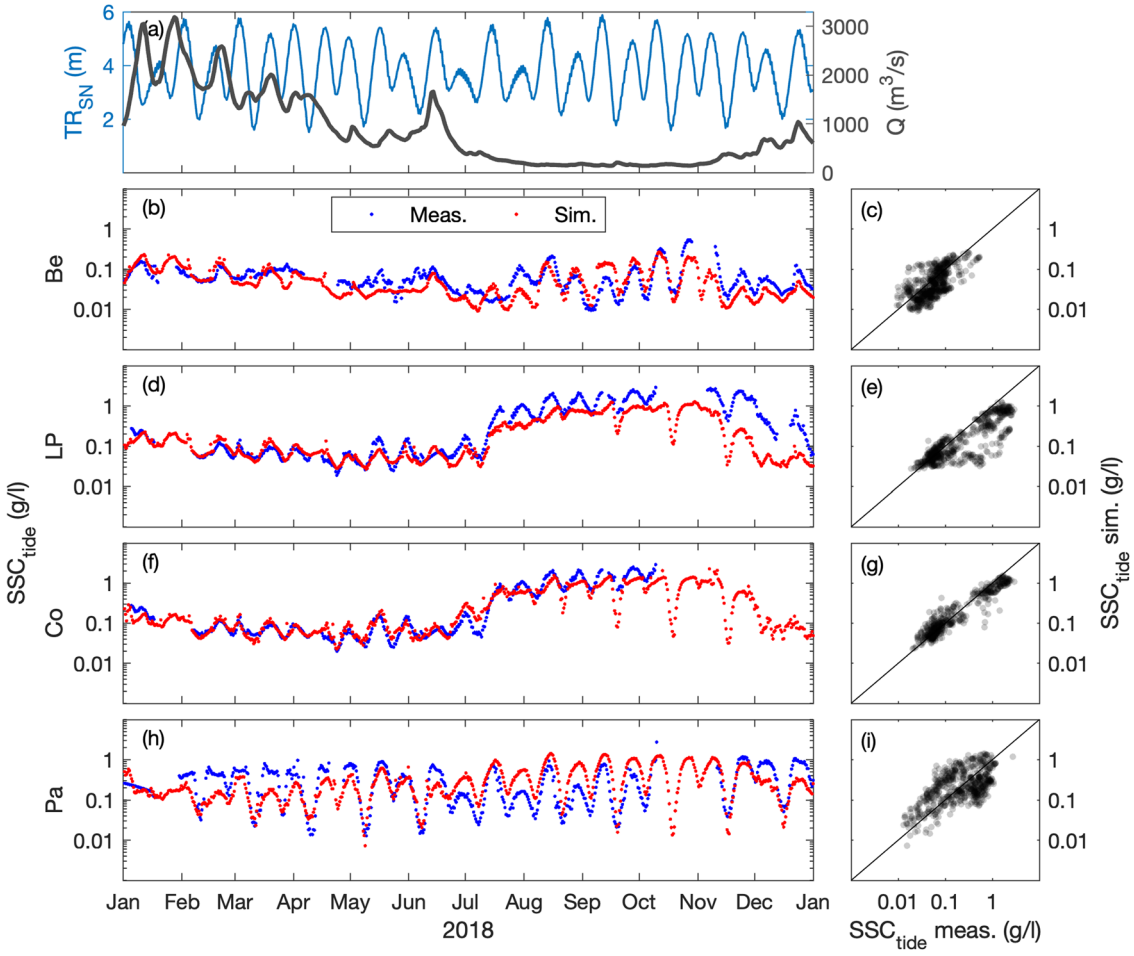

Fig. 10 Hindcast validation of tide-averaged suspended sediment concentration SSC_{tide} along the Loire Estuary. (**a**) Loire River discharge Q at the upstream model boundary and tidal range TR_{SN} at Saint Nazaire 'SN' (blue). Surface SSC_{tide} at (**b,c**) Bellevue 'Be', (**d,e**) Le Pellerin 'LP', (**f,g**) Cordemais 'Co', and (**h,i**) Paimboeuf 'Pa' (see station locations in Fig. 1c). (Left panels) Measurements (blue) and simulations (red), and (right panels) simulations versus measurements, from January to December 2018.

Salinity. The surface salinity (at 1-m below the surface) is compared at Paimboeuf 'Pa' and Le Pellerin 'LP' stations (Fig. 1c), within the maximal salinity gradient area. High-frequency (i.e., every 30 minutes) salinity dynamics are well captured by the model along hydrological cycles (Figs. 5b–e, 6b–e). The model underestimates salinity at Le Pellerin in 2008, but the salinity intrusion during the low river discharge period (i.e., from August to November) is well reproduced. In Figs. 5f–I, 6f–i the tide-averaged salinity comparison further illustrates the model's ability to simulate salinity variations at the hydrological and neap-spring time scales with good skills ($r^2 \geq 0.7$; Table 2).

Suspended sediment concentration. The surface SSC (at 1-m below the surface) is compared at five stations along the estuary, where the turbidity maximum takes place (i.e., Paimboeuf 'Pa', Cordemais 'Co', Le Pellerin 'LP', and Bellevue 'Be'; Fig. 1c). The seasonal and neap-spring variability of high-frequency SSC is reasonably well captured by the model at the different stations, but there is a main underestimation of highly-turbid events (Figs. 7, 8). This is especially visible at the downstream stations during summer (i.e., LP, Co, and Pa). Such underestimations are relatively common in the numerical modelling of estuarine sediment dynamics[53], as monitoring stations along the shore may measure large and local sediment resuspensions that models cannot capture with a 50 to 100 m resolution[21]. However, the model presents better skills at tidal timescales (Table 2), providing confidence in its ability to simulate the main SSC levels along the year (Figs. 9, 10). This is confirmed by the comparison of measured and simulated SSC in function of tidal range and river discharge conditions (Fig. 11). We observe that the model underestimates the SSC at Cordemais and Le Pellerin in 2008 (Fig. 11i,j,m,n), which is not the case in the wetter year 2018 (Fig. 11k,l,o,p). In addition, the model proves to be able to simulate the main tidal and river dynamics.

The model validation of the Loire Estuary hydrodynamics, salinity, and sediment dynamics provides a sufficient level of confidence for using the numerical hindcast in various interdisciplinary studies. However, it is important to acknowledge the model's limitations and errors (Table 2) to properly use the derived environmental

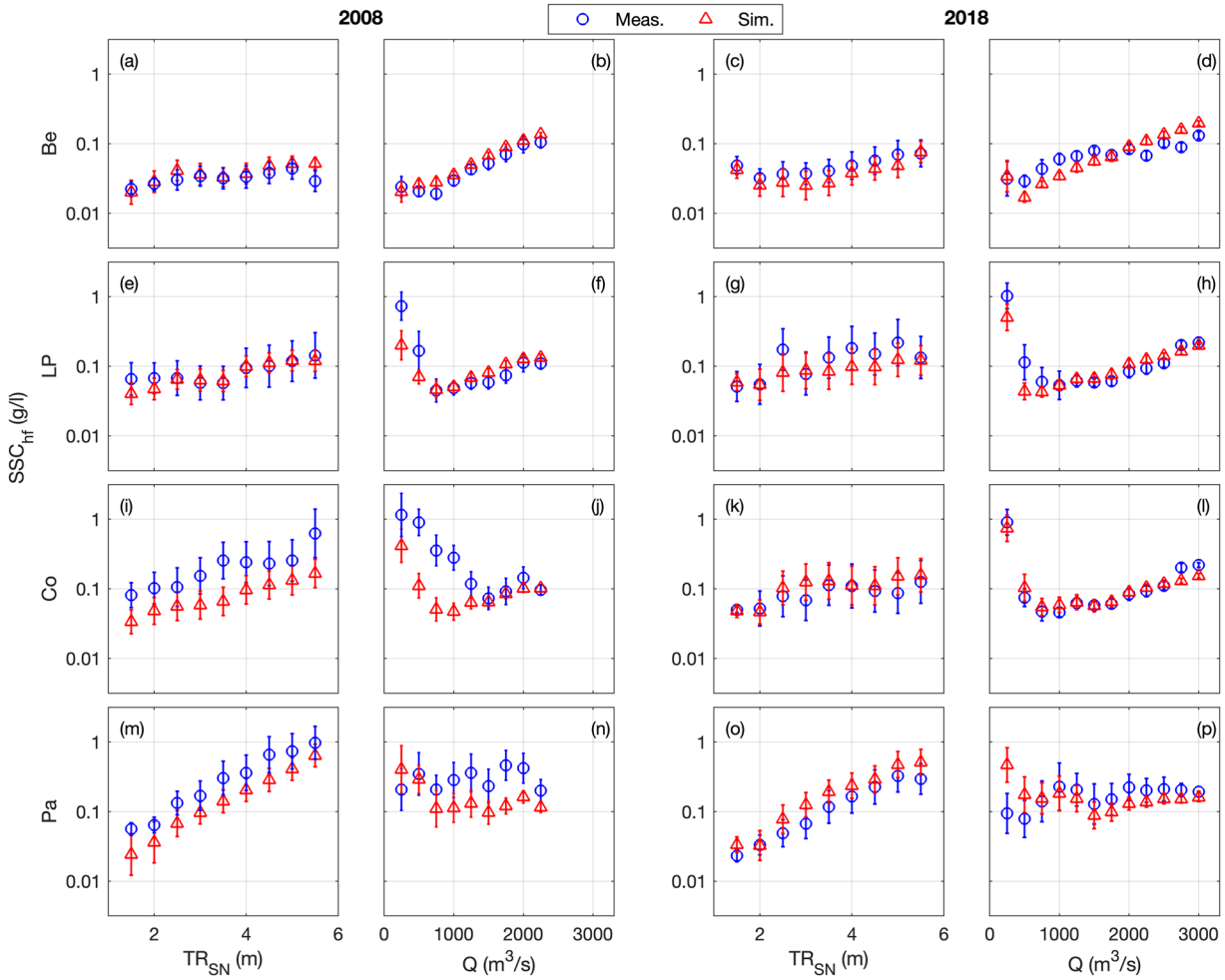

Fig. 11 Hindcast validation of high-frequency suspended sediment concentration SSC_{hf} along the Loire Estuary versus the tidal range TR_{SN} at Saint Nazaire 'SN' and the Loire River discharge Q at the upstream model boundary. Surface SSC_{hf} at (**a**–**d**) Bellevue 'Be', (**e**–**h**) Le Pellerin 'LP', (**i**–**l**) Cordemais 'Co', and (**m**–**p**) Paimboeuf 'Pa' (see station locations in Fig. 1c). Measurements (blue circles) and simulations (red triangles) from January to December 2008 (two left panels) and from January to December 2018 (two right panels). Symbols represent class-averaged SSC_{hf} values (i.e., every 0.5 m for TR_{SN} and every 250 m^3/s for Q), and brackets represent standard deviation.

parameters. For instance, this hindcast provides reasonable estimates of SSC changes in terms of order of magnitude, from tidal to hydrological timescales, but it is associated with greater uncertainties at sub-tidal timescales.

Code availability

The MARS3D-MUSTANG model chain used to provide the hindcast is an open-access software: https://mars3d.ifremer.fr. The source codes and parameter files are available on the CurviLoire Hindcast repository[51].

Received: 15 December 2022; Accepted: 8 June 2023;
Published online: 22 June 2023

References

1. Morris, A., Mantoura, R., Bale, A. & Howland, R. Very low salinity regions of estuaries: important sites for chemical and biological reactions. *Nature* **274**, 678–680 (1978).
2. Avoine, J., Allen, G., Nichols, M., Salomon, J. & Larsonneur, C. Suspended-sediment transport in the Seine estuary, France: effect of man-made modifications on estuary—shelf sedimentology. *Marine Geology* **40**, 119–137 (1981).
3. Le Hir, P. & Thouvenin, B. Mathematical modelling of cohesive sediment and particulate contaminants transport in the Loire Estuary. *OLSEN & OLSEN, FREDENSBORG, DENMARK.*, 71–78 (1994).
4. Sottolichio, A., Le Hir, P. & Castaing, P. Modeling mechanisms for the stability of the turbidity maximum in the Gironde estuary, France. *Proceedings in Marine Science* **3**, 373–386 (2000).
5. Uncles, R. Estuarine physical processes research: some recent studies and progress. *Estuarine, Coastal and Shelf Science* **55**, 829–856 (2002).
6. Sommerfield, C. K. & Wong, K. C. Mechanisms of sediment flux and turbidity maintenance in the Delaware Estuary. *Journal of Geophysical Research-Oceans* **116**, Artn C01005, https://doi.org/10.1029/2010jc006462 (2011).

7. Winterwerp, J. C. Fine sediment transport by tidal asymmetry in the high-concentrated Ems River: indications for a regime shift in response to channel deepening. *Ocean Dynamics* **61**, 203–215 (2011).
8. Bi, Q. & Toorman, E. A. Mixed-sediment transport modelling in Scheldt estuary with a physics-based bottom friction law. *Ocean Dynamics* **65**, 555–587, https://doi.org/10.1007/s10236-015-0816-z (2015).
9. Jalón-Rojas, I., Schmidt, S., Sottolichio, A. & Bertier, C. Tracking the turbidity maximum zone in the Loire Estuary (France) based on a long-term, high-resolution and high-frequency monitoring network. *Continental Shelf Research* **117**, 1–11, https://doi.org/10.1016/j.csr.2016.01.017 (2016).
10. Burchard, H., Schuttelaars, H. & Ralston, D. Sediment Trapping in Estuaries. *Annual review of marine science* **10**, 371–395 (2018).
11. Grasso, F. *et al*. Suspended Sediment Dynamics in the Macrotidal Seine Estuary (France): 1. Numerical Modeling of Turbidity Maximum Dynamics. *Journal of Geophysical Research: Oceans* **123**, 558–577, https://doi.org/10.1002/2017JC013185 (2018).
12. Glangeaud, L. Transport et sédimentation dans l'estuaire et à l'embouchure de la Gironde. Caractères pétrographiques des formations fluviatiles, saumâtres, littorales et néritiques. *Bulletin de la Societe Geologique de France, Paris* **7**, 599–630 (1938).
13. Billen, G. *et al*. A long-term view of nutrient transfers through the Seine river continuum. *Science of the total Environment* **375**, 80–97 (2007).
14. Nichols, F. H., Cloern, J. E., Luoma, S. N. & Peterson, D. H. The modification of an estuary. *Science(Washington)* **231**, 567–573 (1986).
15. Grasso, F., Bismuth, E. & Verney, R. Unraveling the impacts of meteorological and anthropogenic changes on sediment fluxes along an estuary-sea continuum. *Scientific reports* **11**, 1–11 (2021).
16. Grasso, F. & Le Hir, P. Influence of morphological changes on suspended sediment dynamics in a macrotidal estuary: diachronic analysis in the Seine Estuary (France) from 1960 to 2010. *Ocean Dynamics* **69**, 83–100 (2019).
17. Van Maren, D., Van Kessel, T., Cronin, K. & Sittoni, L. The impact of channel deepening and dredging on estuarine sediment concentration. *Continental Shelf Research* **95**, 1–14 (2015).
18. Guo, L. *et al*. A historical review of sediment export–import shift in the North Branch of Changjiang Estuary. *Earth Surface Processes and Landforms* **n/a**, https://doi.org/10.1002/esp.5084 (2021).
19. Jalón-Rojas, I., Schmidt, S. & Sottolichio, A. Turbidity in the fluvial Gironde Estuary (southwest France) based on 10-year continuous monitoring: sensitivity to hydrological conditions. *Hydrology and Earth System Sciences* **19**, 2805–2819, https://doi.org/10.5194/hess-19-2805-2015 (2015).
20. Druine, F. *et al*. *In situ* high frequency long term measurements of suspended sediment concentration in turbid estuarine system (Seine Estuary, France): Optical turbidity sensors response to suspended sediment characteristics. *Marine Geology* **400**, 24–37 (2018).
21. Diaz, M. *et al*. Modeling Mud and Sand Transfers Between a Macrotidal Estuary and the Continental Shelf: Influence of the Sediment Transport Parameterization. *Journal of Geophysical Research: Oceans* **125**, e2019JC015643 (2020).
22. Mengual, B., Le Hir, P., Rivier, A., Caillaud, M. & Grasso, F. Numerical modeling of bedload and suspended load contributions to morphological evolution of the Seine Estuary (France). *International Journal of Sediment Research* (2020).
23. Schulz, E., Grasso, F., Le Hir, P., Verney, R. & Thouvenin, B. Suspended Sediment Dynamics in the Macrotidal Seine Estuary (France): 2. Numerical Modeling of Sediment Fluxes and Budgets Under Typical Hydrological and Meteorological Conditions. *Journal of Geophysical Research: Oceans* **123**, 578–600, https://doi.org/10.1002/2016JC012638 (2018).
24. Lamarque, B. *et al*. Spatial Distributions of Surface Sedimentary Organics and Sediment Profile Image Characteristics in a High-Energy Temperate Marine RiOMar: The West Gironde Mud Patch. *Journal of Marine Science and Engineering* **9**, 242 (2021).
25. Champagnat, J. *et al*. Multidisciplinary assessment of nearshore nursery habitat restoration for an exploited population of marine fish. *Marine Ecology Progress Series* **680**, 97–109 (2021).
26. Lamarque, B. *et al*. Spatiotemporal dynamics of surface sediment characteristics and benthic macrofauna compositions in a temperate high-energy River-dominated Ocean Margin. *Continental Shelf Research* **247**, 104833 (2022).
27. Marchand, J. The influence of seasonal salinity and turbidity maximum variations on the nursery function of the Loire estuary (France). *Netherland Journal of Aquatic Ecology* **27**, 427–436 (1993).
28. Dronkers, J. Convergence of estuarine channels. *Continental Shelf Research* **144**, 120–133 (2017).
29. Winterwerp, J. C., Wang, Z. B., van Braeckel, A., van Holland, G. & Kösters, F. Man-induced regime shifts in small estuaries—II: a comparison of rivers. *Ocean Dynamics* **63**, 1293–1306 (2013).
30. Geyer, W. R. & MacCready, P. The Estuarine Circulation. *Annual Review of Fluid Mechanics* **46**, 175–197, https://doi.org/10.1146/annurev-fluid-010313-141302 (2014).
31. Leuven, J. R., Pierik, H. J., van der Vegt, M., Bouma, T. J. & Kleinhans, M. G. Sea-level-rise-induced threats depend on the size of tide-influenced estuaries worldwide. *Nature Climate Change* **9**, 986–992 (2019).
32. Wei, X. *et al*. Nutrient transport and transformation in macrotidal estuaries of the French Atlantic coast: a modeling approach using the Carbon-Generic Estuarine Model. *Biogeosciences* **19**, 931–955 (2022).
33. Lemoine, J. & Le Hir, P. Maintenance dredging in a macrotidal estuary: Modelling and assessment of its variability with hydro-meteorological forcing. *Estuarine, Coastal and Shelf Science*, 107366 (2021).
34. Lazure, P. & Dumas, F. An external–internal mode coupling for a 3D hydrodynamical model for applications at regional scale (MARS). *Advances in Water Resources* **31**, 233–250 (2008).
35. Roland, A. & Ardhuin, F. On the developments of spectral wave models: numerics and parameterizations for the coastal ocean. *Ocean Dynamics* **64**, 833–846 (2014).
36. Soulsby, R. Dynamics of marine sands: a manual for practical applications. *Oceanographic Literature Review* **9**, 947 (1997).
37. Walther, R., Cayrol, C., Hamm, L., Delouis, A. & Lehay, D. Evaluation of an offshore disposal site in the Loire Estuary through field monitoring and 3D numerical modeling. *Coastal Engineering Proceedings*, 24–24 (2015).
38. Sanchez, M., Grovel, A. & Hosseini, K. Impact sédimentaire des travaux d'aménagement de l'estuaire de la Loire. *Bulletin of Engineering Geology and the Environment* **59**, 239–246 (2000).
39. Khojasteh Pour Fard, I. *Modélisation des échanges dissous entre l'estuaire de la Loire et les baies côtières adjacentes*, Bordeaux, (2015).
40. Grasso, F., Le Hir, P. & Bassoullet, P. Numerical modelling of mixed-sediment consolidation. *Ocean Dynamics* **65**, 607–616 (2015).
41. Le Hir, P., Cayocca, F. & Waeles, B. Dynamics of sand and mud mixtures: A multiprocess-based modelling strategy. *Continental Shelf Research* **31**, S135–S149, https://doi.org/10.1016/j.csr.2010.12.009 (2011).
42. Mengual, B., Le Hir, P., Cayocca, F. & Garlan, T. Modelling fine sediment dynamics: Towards a common erosion law for fine sand, mud and mixtures. *Water* **9**, 564 (2017).
43. Coynel, A. *et al*. Spatial distribution of trace elements in the surface sediments of a major European estuary (Loire Estuary, France): Source identification and evaluation of anthropogenic contribution. *Journal of Sea Research* **118**, 77–91 (2016).
44. Waeles, B., Le Hir, P., Lesueur, P. & Delsinne, N. Modelling sand/mud transport and morphodynamics in the Seine river mouth (France): an attempt using a process-based approach. *Hydrobiologia* **588**, 69–82 (2007).
45. van Leussen, W. *Estuarine macroflocs and their role in fine-grained sediment transport*, University of Utrecht (1994).
46. Migniot, C. Etude des propriétés physiques de différents sédiments très fins et de leur comportement sous des actions hydrodynamiques. *La houille blanche*, 591–620 (1968).
47. Partheniades, E. Erosion and deposition of cohesive soils. *Journal of the Hydraulics Division* **91**, 105–139 (1965).
48. Le Hir, P., Cann, P., Waeles, B., Jestin, H. & Bassoullet, P. in *Proceedings in Marine Science* Vol. 9, 137–153 (Elsevier, 2008).

49. Sanford, L. P. Modeling a dynamically varying mixed sediment bed with erosion, deposition, bioturbation, consolidation, and armoring. *Computers & Geosciences* **34**, 1263–1283, https://doi.org/10.1016/j.cageo.2008.02.011 (2008).
50. Krone, R. B. Flume studies of transport of sediment in estrarial shoaling processes. *Final Report, Hydr. Engr. and Samitary Engr. Res. Lab., Univ. of California* (1962).
51. Grasso, F. & Caillaud, M. CurviLoire Hindcast. *IFREMER*. https://doi.org/10.12770/a56f1a01-bdf2-4f52-9cc7-4e4b8605520c (2023).
52. Guillaud, J. Calcul en temps réel des concentrations fluviales en nutriments, en fonction des débits, sur la façade Atlantique, la Manche et le sud de la Mer du Nord. *RST. DYNECO Pélagos*, 08–05 (2008).
53. van Maanen, B. & Sottolichio, A. Hydro-and sediment dynamics in the Gironde estuary (France): Sensitivity to seasonal variations in river inflow and sea level rise. *Continental Shelf Research* **165**, 37–50 (2018).

Acknowledgements

This work has been carried out in the framework of the CAPTURE project within the "Inter-estuary Mission" (MIE) funded by the French Biodiversity Agency (OFB). The authors would like to acknowledge the *Groupement d'Intérêt Public Loire Estuaire* for providing the measurements used in the model validation (i.e., *in-situ* data from the SYVEL high-frequency monitoring network).

Author contributions

M.C. mainly contributed to the configuration and deployment of the MARS3D and WAVEWATCH III® models. F.G. contributed to the configuration and deployment of the MUSTANG model and wrote the main part of the manuscript.

Competing interests

The authors declare no competing interests.

Additional information

Correspondence and requests for materials should be addressed to F.G.

Reprints and permissions information is available at www.nature.com/reprints.

Publisher's note Springer Nature remains neutral with regard to jurisdictional claims in published maps and institutional affiliations.